AERODYNAMIC DESIGN AND ANALYSIS OF AN INNOVATIVE REGIONAL TURBOPROP CONFIGURATION

Fabrizio Nicolosi*, Salvatore Corcione*, Pierluigi Della Vecchia*, Vittorio Trifari*, Manuela Ruocco*,
***University of Naples Federico II, Department of Industrial Engineering, Aerospace Division**

Keywords: *Aircraft Design, Aerodynamic analysis, Winglet, High Lift Devices, CFD analysis*

Abstract

The Innovative turbopROp configuratioN (IRON) project complies with the European Union topic JTI-CS2-2015-CPW02-REG-01-03 (Green and cost efficient Conceptual Aircraft Design including Innovative Turbo-Propeller Power-plant) as part of the Clean Sky 2 program for Horizon 2020. The topic leader is Leonardo, CIRA (Italian Aerospace Research Center) is the coordinator and several core-partners are involved into the project. The research work is focused on the feasibility study of an innovative turboprop aircraft configuration with rear engines installed on the horizontal tailplane.
This paper deals with the aerodynamic design and analyses carried out during the first loop of design concerning the baseline configuration provided by Leonardo Company.
Major activities have been addressed to the design of the wing airfoil and to an efficient high lift system (including the possibility of a morphable drooped nose). Winglets have been specifically designed to improve the climb performance concurrently reducing the induced drag in cruise condition.
The complete aerodynamic database assessment has been performed also by means of high fidelity analyses, such as CFD-RANS simulations, to estimate the isolated wing high lift capabilities (flap up and flap down) and the fuselage aerodynamic characteristics. To assess the complete aircraft trimmed drag polar database, a detailed weight and balance analysis has been performed. This analysis has shown that for this innovative configuration, the center of gravity excursion is very large, highlighting the inadequate sizing of the horizontal tailplane to trim the aircraft in the whole center of gravity excursion range.
To overcome this issue, different aircraft configurations have been considered. Among them also three lifting surfaces has been considered. This latter has been identified as the most promising solution to best comply with the provided aerodynamic requirements.

1 Introduction

The IRON project is focused on the feasibility study of an innovative turboprop regional configuration. The research addressed to the analysis and design of this innovative regional platform will be developed through three different loops with increasing level of complexity and fidelity (see Fig. 1). The aircraft configuration will be assessed through numerical simulations during the first and second design phase, and experimental validations will be performed during the third loop, so that at the end of the project a Technology Readiness Level (TRL) 4 will be reached.
The loop 1 started in July 2016 from the baseline configuration provided by Leonardo Company and ended in January 2017. The aircraft under investigation is an innovative layout with low wing. Engines are rear installed on the horizontal tail tips as shown in Fig. 2.
Top Level Aircraft Requirements (TLAR) have been issued by Leonardo company, which also provided the aircraft maximum takeoff weight and wing area.
TLAR are very challenging: a cruise Mach number of 0.62 at 30000 feet, with a moderately maximum lift coefficient and low drag to achieve

a cruise aerodynamic efficiency about 18. In particular, a maximum lift coefficient of 2.4 and 3.0 in take-off and landing conditions are respectively required. Moreover, it is expected that the inner wing airfoils have 18% relative thickness to reduce the wing weight and to allow the landing gear to be stored within. A summary of the main TLAR is reported in Table 1, while in Table 2 some of the main dimensions are illustrated.

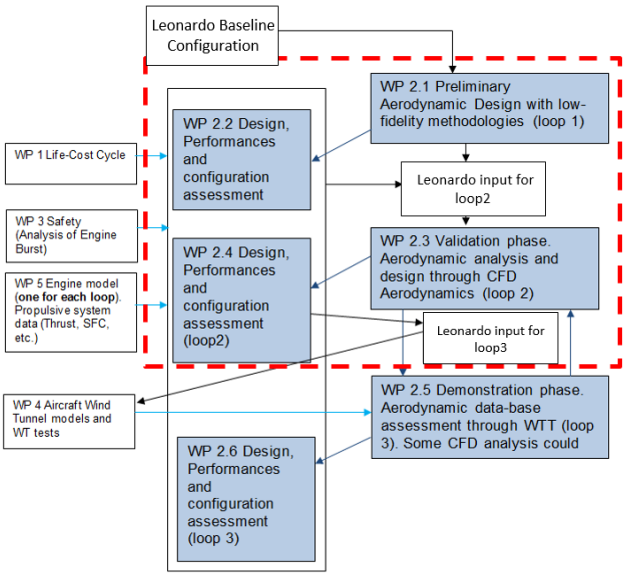

Fig. 1 IRON project loops

	Metric	Imperial
PAX	From 110 to 130pax	
Design range	2960km	1600 nm
Cruise speed	M 0.62@FL300	
OEI ceiling @ 97% MTOW, ISA +10	> 5030m	> 16500ft
TOFL (ISA, SL, MTOW)	< 1400m	< 4600ft
LFL (ISA, SL, MTOW)	< 1300m	< 4265ft
Fuel reserves	5%	100nm
Cruise efficiency	18@FL300	
C_{Lmax} landing	3.0	
C_{Lmax} take-off	2.4	

Table 1 Top Level Aircraft Requirements

The present paper deals with the activities performed by the Design of Aircraft and Flight Technologies (DAF) research group at UNINA[1] during the first design loop. The research group is the leader o aerodynamics and performance work package of the IRON project (see Fig. 1).

	Metric	Imperial
Fuselage diameter	3.54 m	139 in
Fuselage length	38 m	124.7 ft
Wing planform area	105 m^2	1130.2 ft^2
Wing leading edge sweep angle	10 deg.	
Horizontal tail planform area	33 m^2	354.1 ft^2

Table 2 Aircraft baseline geometric data.

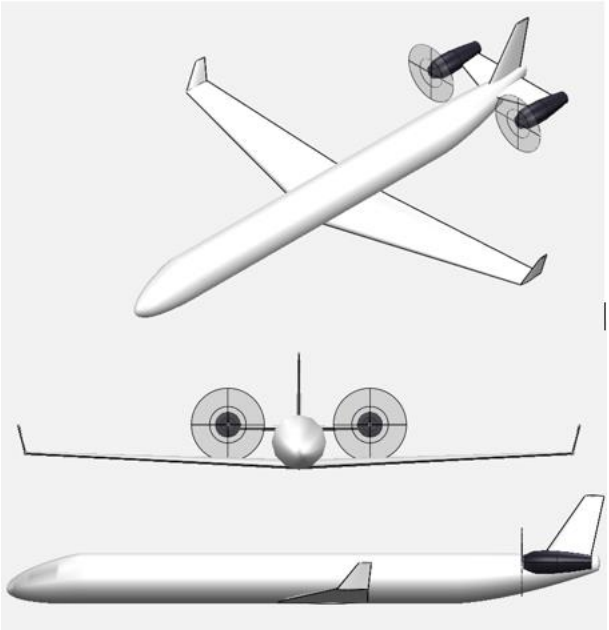

Fig. 2. IRON aircraft baseline

DAF group during the last years, has been involved in many numerical and experimental aerodynamic design and analyses[1][2][3][4], growing large experience in designing and optimizing of regional turboprop aircraft[5][6][7]. Reliable design methodologies have been developed through numerical and experimental tests[8][9], and applied to the design and analysis of light, general aviation and turboprop aircraft[10][11][12]. Moreover, all the developed methodologies have been integrated within a standalone Java library, dedicated to the design and optimization of transport aircraft[13][14]. All the collected knowledge, tools and methods, have been applied in the design and analysis of the IRON project aircraft. The aerodynamic analysis, and thus the structure of this paper, has been broken down in the following topics:

- Airfoil and high lift devices design, shown in section 2. As previously stated, this task was challenging because of the high

[1] http://www.daf.unina.it

aerodynamic efficiency required having an airfoil with 18% of thickness. Natural laminar flow was mandatory to comply with TLAR. Moreover, the airfoil should provide acceptable aerodynamic characteristics also in fully turbulent flow. Once the wing airfoil has been defined an efficient fowler flap has been designed. To improve the landing maximum lift coefficient, the effects of a droop nose has been also evaluated. To assess the wing maximum lift capabilities, a 3D isolated wing CFD analyses have been performed.

- Winglets have been specifically designed to reduce the induced drag improving mainly the climb performance. Results of this task are shown in section 3.
- Fuselage aerodynamic characteristics have been estimated through several methods, including CFD-RANS analyses.
  Results and comparisons between the applied methods are illustrated in section 4.
- A detailed weight and balance analyses has been performed to assess the design and sizing of the baseline configuration.
  Results are shown in section 5. This task has highlighted some criticalities of such a configuration dealing with the center of gravity excursion which resulted to be very wide (from 4% to 52% of the mean aerodynamic chord). Due to this issue, a review of the aircraft configuration and sizing has been done.
- According to the weight and balance estimation, at the beginning of the Loop 2, the baseline configuration has been revised (regarding wing position, horizontal tail area, and so on.) to ensure stability and control for each considered center of gravity excursion. Three solutions have been investigated, considering also a three lifting surfaces configuration. Results are shown and discussed in section 7.

2 Airfoil and High Lift Devices

To comply with the challenging TLAR provided by Leonardo Company for the IRON project, a specific wing airfoil has been conceived. To define the operating conditions at which the airfoil must be designed, a preliminary wing aerodynamic analysis has been performed by means of the ADAS software (Aircraft Design and Analysis Software), developed by DAF group[7][15]. The clean wing (flap up) analysis is based on the Vortex Lattice Method (VML)[13][14], while for the maximum lift coefficient prediction in both flap up and flap down conditions semi-empirical approaches like those suggested by Roskam and Sforza[16][17] have been applied.
Wing span loading at cruise conditions is illustrated in Fig. 3. In this latter, the three red lines highlight the cruise lift coefficients of the main wing sections at which the wing airfoils should provide the minimum drag.
NACA laminar airfoils have been chosen as baseline of this analysis.

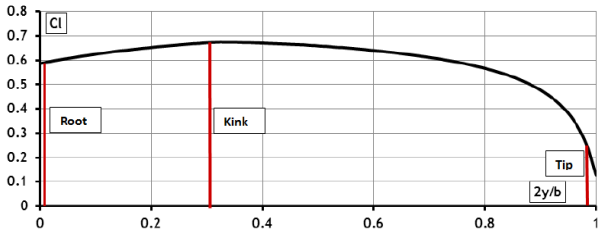

Fig. 3 Wing span loading M=0.62 @FL300 and wing A.o.A = 2°.

The wing lift curves in clean and landing flap condition are shown in Fig. 5.
A sensitivity analysis has been carried out to assess optimum values for flap chord ratios and for flaps spanwise extension.
To reach the target maximum lift coefficient of 3.0 in landing condition, the use of a single slot fowler flap turns out to be not sufficient. Thus, a leading edge high lift device should be considered. However, to preserve the wing laminar flow, a morphable droop nose has been considered.
A sketch of the wing planform including high lift devices is illustrated in Fig. 4.

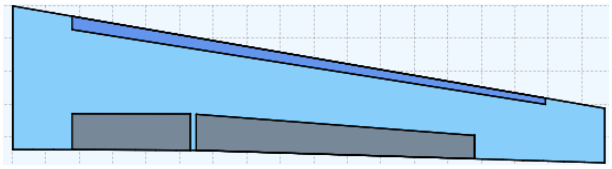

Fig. 4 Wing High-Lift Devices sketch.

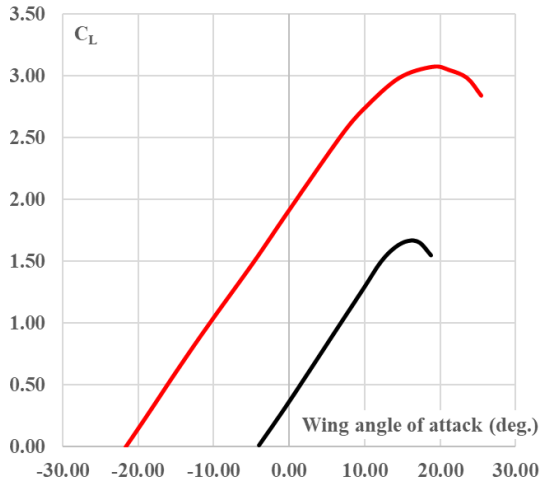

Fig. 5 Wing lift curve: flap up (black line), flap and slat at landing condition (red line).

2.1. 2D Airfoil Design

The wing airfoil design has driven by three major conditions as illustrated in Fig. 6.
To match the cruise efficiency, a laminar airfoil was required, avoiding any drag increase deriving from strong shock waves (Target A of Fig. 6). To reach the prescribed wing maximum lift coefficient, airfoils themselves must have a moderately high maximum lift coefficients (Target B of Fig. 6). Finally, in order to avoid a large decay of the aerodynamic performance, the off-design conditions must be checked (Target C of Fig. 6). Moreover, aircraft requirements fixed the wingspan thickness: root and kink sections must have a relative thickness of 18% and the tip realtive thickness is 14%.
The airfoil design has been accomplished by means of the inverse design routine of MSES software, by modifying the pressure coefficient distribution until the desired aerodynamic characteristics have been reached. The inverse design started from the NACA 66(3)-418 reference airfoil and was focused on the kink airfoil because this is the most relevant wing section. The designed airfoil is compared witht the reference airfoil in Fig. 7. For the second design loop, once the aircraft configuration and sizing will be well assesed, the airfoil will be optmized by means of dedicated tools (i.e. geometry parametrization coupled with optimization alghoritms based on computational intellingence). MSES has been the main tool used to investigate the aerodynamic characteristics of the airfoil (in particular to evaluate the lamianar drag bucket and the minimim drag coefficient). The cruise kink airfoil drag polar in both free transition and fully turbulent conditions is illustrated in Fig. 8.

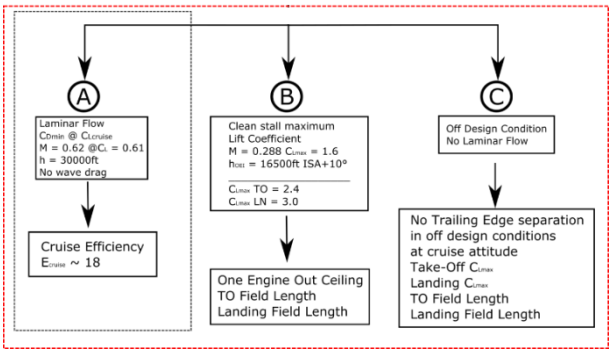

Fig. 6 Scheme of the airfoil targets for its design.

Fig. 7 Kink airfoil: comparison with the reference NACA laminar airfoil.

The laminar drag bucket is spread over a wide range of lift coefficient showing its minimum (40 drag counts) at the cruise lift coefficient of about 0.6-0.7. Thanks to this characteristic, the wing tip airfoil can be derived from the kink section. In particular, the kink airfoil thickness has been adequately scaled and its camber has been reduced to center the minimum drag at the required lift coefficient.
A minimum drag coefficient of about 40 drag counts (which is 20/25 drag counts lower than a non-laminar airfoil having the same thickness) is the minimum value to reach the wing parasite drag that comply with the prescribed aircraft cruise efficiency.
The high lift characteristics in clean configuration have been also assessed by means of high-fidelity tools such as a RANS (Reynolds Average Navier Stokes) solver. The comparison between the MSES prediction and the RANS results are shown in Fig. 9.
To reach a minimum drag coefficient that comply with the required cruise efficiency, the laminar

flow extension on the upper side of the airfoil should be about 47% to 50% of the chord, as it is illustrated in Fig. 10.
This latter, coupled with the maximum high lift coefficient, has leaded to an airfoil having a high camber in the trailing edge area. This affects the pitching moment coefficient which results to be about Cm_{ac} = -0.16 in cruise conditions. This takes a toll to meet all the aerodynamic targets complying with wing thickness distribution constraint.

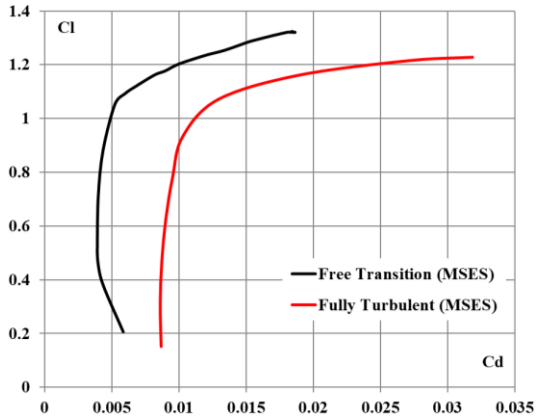

Fig. 8 Cruise drag polar: free transition (black line) and fully turbulent (red line).

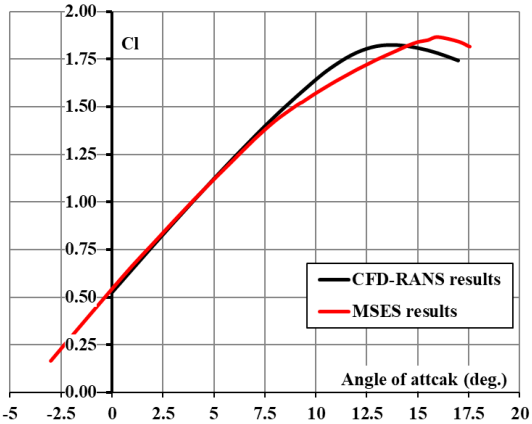

Fig. 9 Airfoil lift curve in stall condition: MSES (red line) vs. CFD-RANS (black line).

Designing the airfoil, a safety margin about the cruise lift coefficient at which the drag divergence occurs has been considered to account for possible gusts.
As it is shown in Fig. 11, the airfoil exhibits no wave drag (no strong shock waves) until a lift coefficient of about 0.9.
The design of the fowler flap has been performed for three different wing sections: the inner, the kink and the outer one, see Fig. 12.

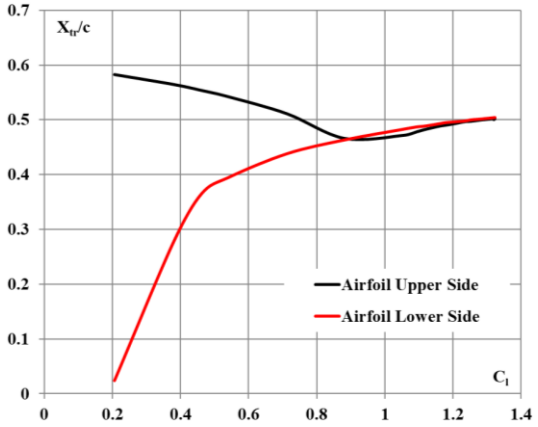

Fig. 10 Kink airfoil, non-dimensional transition abscissa, MSES results.

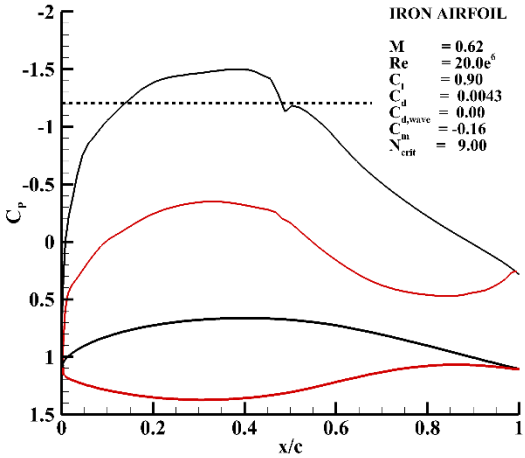

Fig. 11 Kink airfoil: pressure coefficient in cruise condition, (MSES).

This has been necessary because those three sections, according to the preliminary sizing of the high lift system, have three different flap chord ratios, as illustrated in Table 3.
The flap slot, the flap shape, the right gap and overlap values have been designed considering the suggestions available in literature regarding similar airfoils[18]. Once the flap slot and the flap shape have been conceived, its best positioning in terms of gap and overlap values has been identified by means of "airset" routine of the MSES software.
This routine allows the user to deflect and move the flap with respect to an assigned point. Several values of gap and overlap have been investigated, choosing the ones that provide for the highest maximum lift.

Sec.	2y/b	cf/c	Take-Off		Landing	
			M	Re	M	Re
Inner	0.11	0.27	0.171	$16.2e^6$	0.154	$14.5e^6$

Kink	0.30	0.32	0.171	$17.7e^6$	0.154	$16.0e^6$
Outer	0.78	0.32	0.171	$8.8e^6$	0.154	$7.8e^6$

Table 3: Flap sections data.

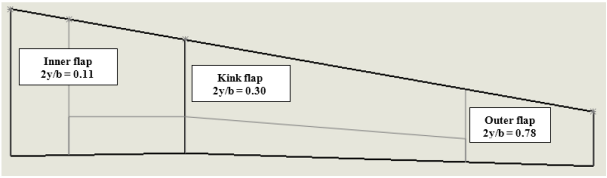

Fig. 12 High lift devices wingspan position.

The optimum flap shape, and gap and overlap values for an assigned deflection, has been chosen to place the expansion peak of the pressure coefficient almost at the exit of the slot. In this way it is possible to maximize the flow acceleration avoiding the flow separation on the flap. An example of this procedure is illustrated in Fig. 13.

Fig. 14 shows the chosen flap positions for the kink section. Flap deflection of 15° and 35° have been selected for take-off and landing condition respectively.

Fig. 15 shows the comparison between the lift curves carried out by means of the MSES code and CFD-RANS calculations.

An example of velocity magnitude contour, calculated using a CFD-RANS simulation in take-off conditions is shown in Fig. 16. Same results are shown in Fig. 17 and Fig. 18 where the kink flap section has been analyzed at landing condition.

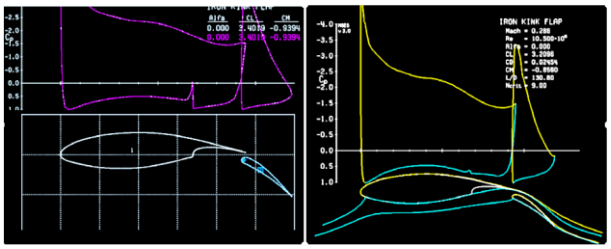

Fig. 13 Example of flap positioning by means of "airset" routine of the MSES software.

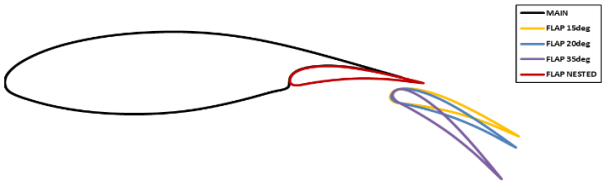

Fig. 14 Fowler flap design: kink section flap at several deflections.

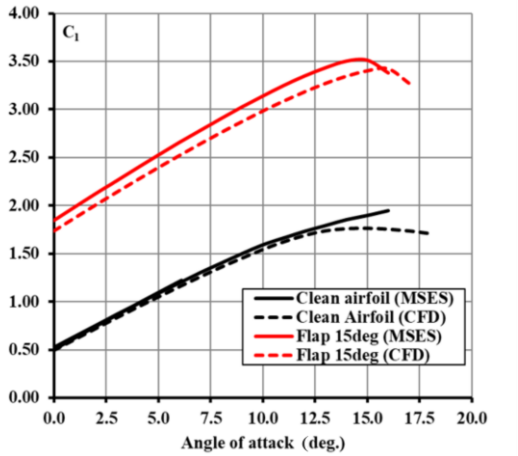

Fig. 15 Fowler flap design: flap 15 deg. MSES vs. CFD, M=0.17 Re=$13.7e^6$.

The same numerical analyses have been accomplished also for the inner and outer flap sections, to produce a complete dataset for a semi-empirical approach of the 3D maximum lift prediction.

A preliminary investigation about the effects of a droop nose has been performed. In the case of such a leading-edge device, the benefit of the smart droop nose comes from a smooth surface without gaps and steps. Following some suggestions that can be found in literature [19], a first attempt of a simplified droop nose geometry has been drawn and analyzed by means of CFD RANS solver.

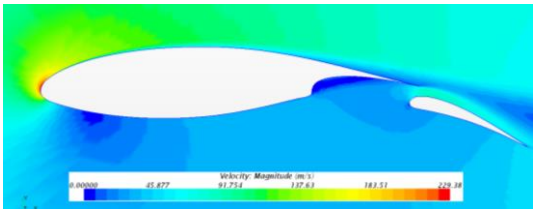

Fig. 16 Fowler flap design: flap 15 deg. CFD velocity magnitude contour, M=0.17 Re=13.7e6 alpha = 15°.

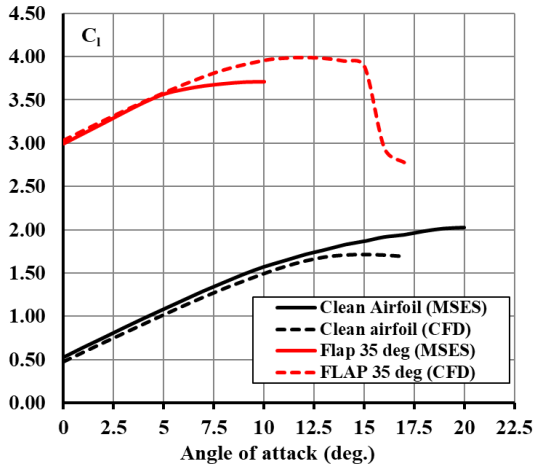

Fig. 17 IRON fowler flap design: flap 35 deg. MSES vs. CFD, M=0.15 Re=12.3e6.

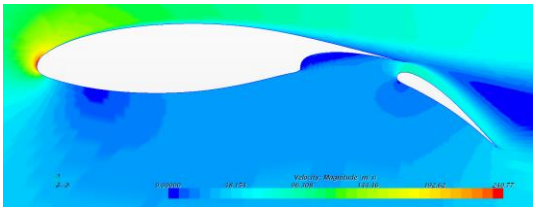

Fig. 18 CFD velocity magnitude contour, M=0.15 Re=12.3e6 alpha = 13°.

The simple droop nose geometry here investigated is obtained by rotating the airfoil coordinates with respect to a point located on the lower airfoil surface at x/c=0.15. This design is a simplification of the droop nose geometry that can be found in[19], where both numerical CFD and experimental wind tunnel tests have been performed to evaluate the effects of droop nose on high lift characteristics of a high efficiency laminar wing.

In this preliminary investigation, at take-off condition, a deflection of 15° of the droop nose has been considered. For the landing configuration the droop nose deflection should be higher than 15°, as suggested in[19], where the best combination found is 25°. of droop nose with 35°-40°. of flap angle. Thus, at landing condition, a droop nose deflection of 25°has been selected. Fig. 19 shows the high lift devices arrangement considered for this preliminary analysis.

Fig. 19 Kink section: take-off (black line) and landing (red line) high lift devices configuration.

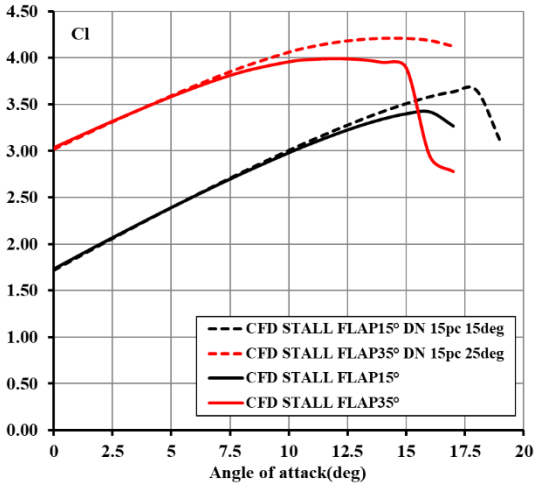

Fig. 20 Kink flap section: droop nose effects on lift coefficient, CFD results.

In Fig. 20 the effects of the droop nose on the lift curve are illustrated as regards the wing kink section (the same analyses have been performed also for the inner and outer flap section). The droop nose delays the stall and increases the maximum lift coefficient. A droop nose deflection of 15° (considered for the take-off condition) increases the maximum achievable lift coefficient around 0.2 in average for each wing section. The same increment of maximum lift coefficient can be found for 25° droop nose deflection with 35° of flap (landing configuration) (see Fig. 19).

The pitching moment coefficient seems not to be significantly affected by the droop nose deflection. At high lift coefficients (or high angle of attack), the droop nose reduces the drag coefficient. This occurs when the flow angle is aligned with the drooped leading edge, reducing the adverse pressure peak. Similar results in terms of pitching moment and drag coefficient variations can be found in[19].

2.2. 3D Wing High Lift Analysis

The wing high lift prediction has been accomplished through the semi-empirical approach suggested by Sforza[17]. This approach requires 2D maximum lift coefficient increment produced by the flap deflection. Although the semi-empirical approach provides the estimation of 2D flap section data, for a more reliable 3D estimation, 2D high-fidelity CFD analyses (shown in section 2.1) have been used.

The isolated 3D wing high lift capabilities have been also checked by means of RANS calculations as shown in Fig. 22 to Fig. 24, where the comparison between the semi-empirical prediction (based on 2D CFD data, the blue line of Fig. 22 and Fig. 23) and the complete 3D RANS simulations are illustrated for clean, take-off and landing conditions. For take-off, a flap deflection of 15° has been assumed and no droop nose augmentation is required (CL_{MAX_TO} = 2.65).
Maximum landing lift coefficient for the isolated wing is shown in Fig. 23, providing a CL_{MAX_LND} = 3.25.

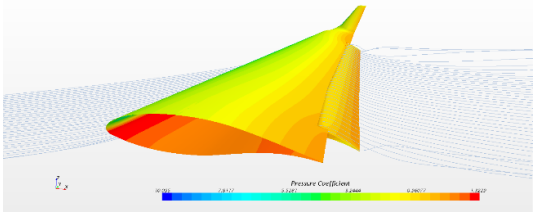

Fig. 21 Isolated Wing: flap =15°, alpha = 10°.

The 3D semi-empirical approach returns a C_{Lmax} lower than the CFD analysis. This methodology provides a correction factor that accounts for a non-optimized flap deflection. According to the methodology, the optimum fowler flap deflection is 40°, thus, for any other flap position, a correction factor is applied. This latter reduces both maximum lift coefficient and stall angle of attack. The fowler flap design, here presented, has been optimized for both take-off and landing positions. So, the correction factor should not be applied for these two configurations.

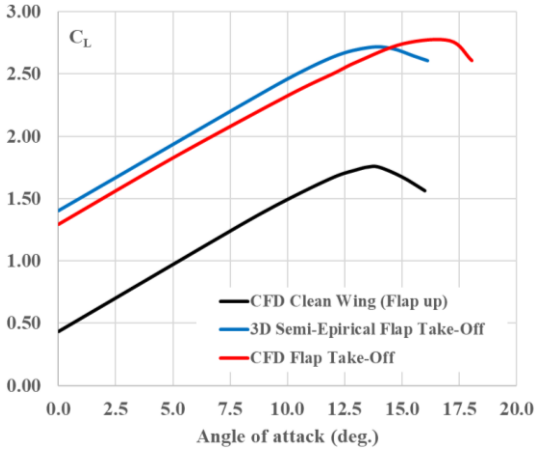

Fig. 22 Isolated Wing: flap 15°, CFD vs. Semi-empirical 3D prediction.

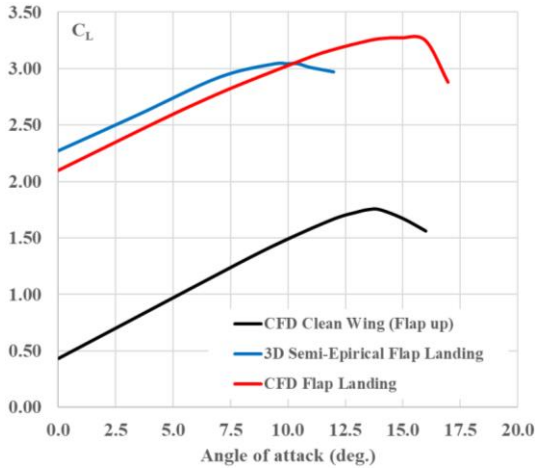

Fig. 23 Isolated Wing: flap 35°, CFD vs. Semi-empirical 3D prediction.

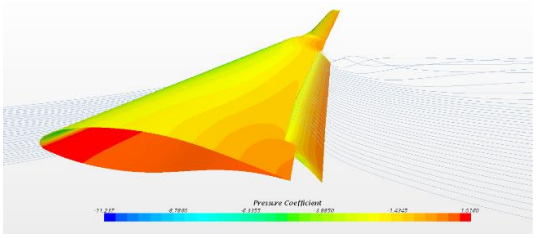

Fig. 24 Isolated Wing: flap 35°, alpha = 10°.

3 Winglet design

The winglet design has been accomplished by means of an in-house developed tool by UniNa DAF research group. The code, developed in MATLab® language, allows to generate a winglet shape starting form a reference wing geometry and assigning several winglet design parameters (such as cant angle, toe angle, winglet height, winglet airfoil, etc.). Then an automated

procedure performs aerodynamic calculations by means of 3D panel code.
The best winglet shape has been carried out through the evaluation of several designs defined as the combination of the following parameters:

- Winglet height (h_w)
- Winglet sweep angle (Δ_w)
- Cant angle ($cant_w$)

These can be considered the major drivers in the winglet design because their definition involve both wing aerodynamic and structural aspects. In general, structural reasons impose a maximum winglet height close to 10% of wing semi-span. The range of variation for Δ_w is linked to the wing sweep angle in order to preserve a sort of continuity in geometrical shape. A range for cant angle ($cant_w$) is assumed considering the same maximum wing span of the reference wing. The wing tip airfoil scaled to a thickness ratio equal to 11% has been assumed as winglet airfoil.
The parameter here used to evaluate each of the analyzed winglet shape is the wing-induced drag factor e_w.
In Fig. 25 examples of winglet parametric designs are illustrated. The effects of each of the design parameters on the wing induced drag factor (percentage variation with respect to the reference value) are shown from Fig. 26 to Fig. 28.
To limit the increase of the wing root bending moment due to the additional load at the wing tip introduced by the winglet, the height of this latter has been fixed to 1.4 m. Moreover, as it can be appreciated in the chart of Fig. 26, there is no sensitive increase of the induced drag factor with a further increase of the winglet height. Winglet sweep angle seems to have no effects on the wing induced drag factor (see Fig. 27). A sweep angle of 55° has been selected only to preserve the wing leading edge shape. The winglet cant angle has been selected to reach the maximum increase of the induced drag factor. As it is shown in Fig. 28, this value is about 85°. It must be highlighted, that the wing-winglet configuration have the same span of the reference wing.
The main aerodynamic effects of such a wing tip device is to improve the climb performance (in particular the rate of climb and ceiling in One Engine Inoperative condition).
The wing drag variation due to the winglet is illustrated in Fig. 29. Here can be appreciated how the break heaven point can be found at C_L = 0.41. In this particular case, the aircraft lift cruise coefficient is about 0.61, this means that winglet can reduce the wing drag also in cruise condition. As shown in Fig. 29, at C_L = 0.61 winglet can reduce the drag coefficient of about 6 drag counts.

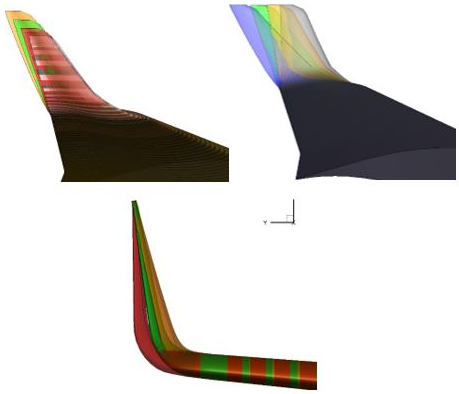

Fig. 25 Winglet design: parametric shapes.

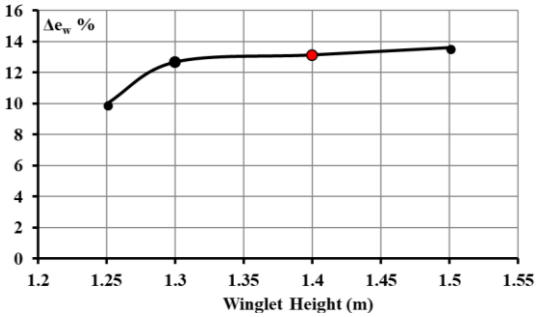

Fig. 26 Effects of winglet height on e_w.

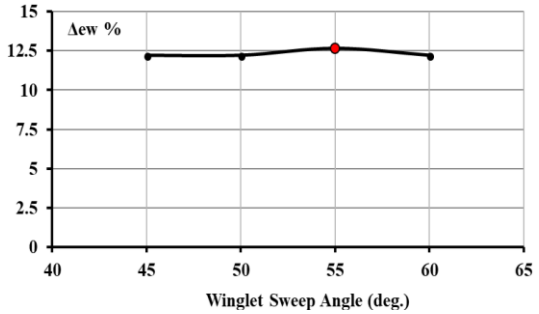

Fig. 27 Effects of winglet sweep angle on e_w.

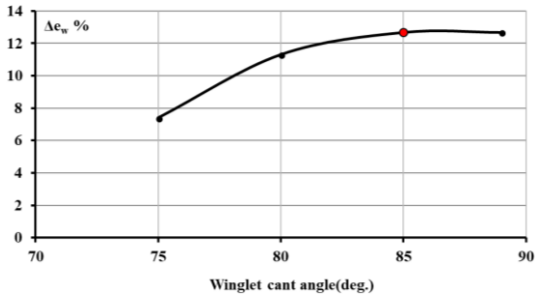

Fig. 28 Effects of winglet cant angle on e_w

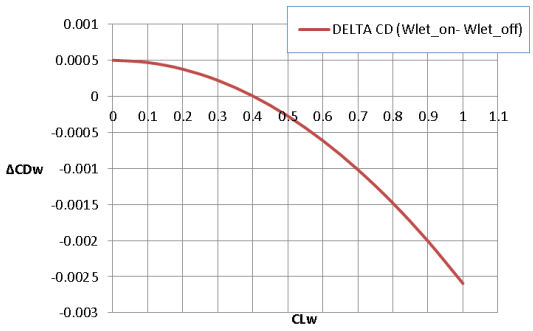

Fig. 29 ΔC_{DW} due to the winglet (M=0.3, Re=13e^6).

4 Fuselage Aerodynamics

The fuselage aerodynamics has been investigated through several approaches:

- Semi-empirical approach suggested by Perkins[20]
- Munk and Multhopp theory[21][22] applied through the strip method suggested by Perkins[20]
- RANS fully turbulent flow simulation (Star-CCM+ simulations)
- FusDes, method developed at the Industrial Engineering Department of UNINA[8]

The first two approaches lead to the estimation of the fuselage longitudinal and directional stability characteristics. RANS simulation allows also the estimation of the fuselage drag and the FusDes method allows the calculation of both longitudinal and directional stability characteristics also providing an estimate of the C_{Do}.

In **Errore. L'origine riferimento non è stata trovata.** the coefficients that can be estimated by applying the selected approaches are summarized. As it can be seen from data in the table the semi-empirical approach (Perkins) is quite far from results achieved by all the other approaches, while both strip theory, RANS and the FusDes method are quite in line except for the C_{Mo}.

Method	C_{Mo}	$C_{M\alpha}$ (deg^{-1})	$C_{N\beta}$ (deg^{-1})	C_{Do}
Perkins	-0.062	0.053	0.003	---
Strip Theory	-0.147	0.028	0.003	---
CFD	-0.026	0.027	0.002	0.008
FusDes	-0.020	0.024	0.002	0.007

Table 4 Fuselage aerodynamics.

5 Weight and Balance

The final output of the aerodynamic database assessment is the complete set of trimmed drag polar curves at main flight conditions. To achieve this task, the estimation of the most forward and most aft position of the aircraft center of gravity is needed. With respect to the center of gravity excursion the horizontal stabilizer must be adequately sized.

The aircraft weights breakdown has been accomplished according to Torenbeek's methodology[23] also considering suggestions coming from Leonardo Company concerning the mass estimate of wing, fuselage, horizontal tail and systems of such an innovative configuration. Weight and balance, stability analysis and trimmed drag polar have been calculated by the means of JPAD software developed at DII[13][14]. Table 5 shows the major aircraft masses breakdown. Starting from the empty mass and its relative center of gravity position, the aircraft load and balance diagram has been calculated (cabin fuselage arrangement provides for a 5 abreast configuration). The load and balance diagram of the reference aircraft is shown in Fig. 30. As it can be seen from that chart, the center of gravity excursion is very large, from 4% to 52% of the mean aerodynamic chord.

This wide center of gravity shift leads to a large variation in the static stability margin. The large stability margin in the most forward center of gravity position entails significant trim drag because a center of gravity position well forward

of the neutral point must be counteracted by a large download on the tail, resulting in a lower maximum lift coefficient (flap down). Also, the cruise efficiency will be significantly affected by this large center of gravity shift.

Component	Mass (kg)
Wing	6181
Horizontal Tail	1210
Vertical Tail	705
Fuselage	8176
Undercarriage	2141
Engines&Nacelles	6065
Systems Overall	5987
Operating Item Mass	1120
OEW	33681
MZF	50111
Payload	14040
MTOW	54428

Table 5 Reference Aircraft Weights Breakdown.

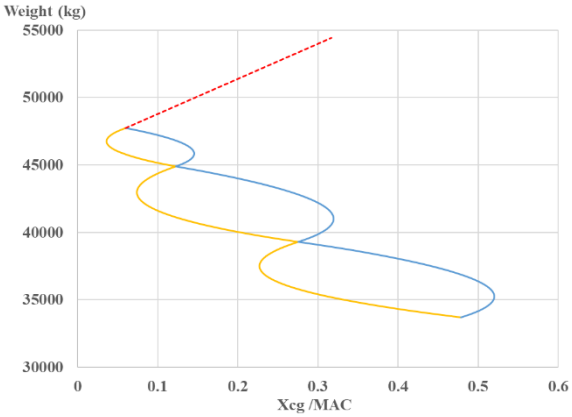

Fig. 30 Baseline aircraft load and balance diagram.

Once the limits of the load and balance diagram have been determined, a complete aircraft stability analysis has been performed. The aircraft stability has been checked in the most aft center of gravity position (the most critical condition), while the aircraft cruise efficiency (the TLAR target is 18 at $C_{L,cruise}$ = 0.61 at FL300) and the take-off and landing C_{Lmax} have been evaluated in the most forward center of gravity position (the most unfavorable condition for the tail download).
In this case, the cruise efficiency is about 16.7, well below the required target of 18. The maximum take-off and landing lift coefficients result to be 2.15 and 2.30 respectively (the assigned targets are 2.4 and 3.0, see Table 6).

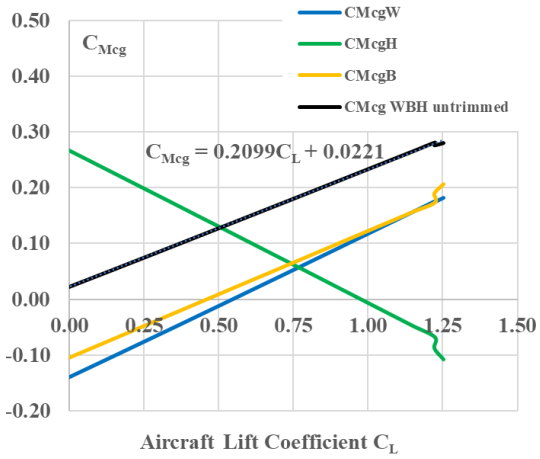

Fig. 31 Baseline C_{Mcg} breakdown, X_{cg} = 52%MAC, M=0.62 @FL300.

Those results highlight how the baseline configuration design and sizing must be revised to meet the TLAR.

6 Aircraft Configuration Revision

Section 5 has highlighted that the baseline aircraft configuration must be revised to meet the aerodynamic targets.
In this section a summary of the preliminary design and sizing analyses, carried out at the end of the first design loop, are illustrated.
Three different aircraft configurations are here discussed:

1. Configuration 1 with the minimum limitations on the center of gravity shift;
2. Configuration 2 with heavy limitations to aircraft operational flexibility;
3. Configuration 3 with three lifting surfaces and a minimum limitation of the center of gravity shift.

All configurations have been designed following the same procedure: *i)* semi-empirical methodologies, implemented in JPAD software[13][14], have been used to analyze a large number of configurations generated by varying several design parameters (wing position, wing area, wing sweep angle, horizontal tail area, horizontal tail aspect ratio, and so on); *ii)* results of those analyses have been used to build up response surfaces useful for an

optimization process; *iii)* configuration optimization.

The optimization process has been accomplished by means of the MOEA Framework which is a free and open source Java library for developing and experimenting with multi-objective evolutionary algorithms (MOEAs), and other general-purpose computational intelligence. Here the ε-NSGAII and OMOPSO algorithms are used. ε-NSGA-II is an extension of NSGA-II that uses an ε-dominance archive and randomized restart to enhance search and find a diverse set of Pareto optimal solutions. Full details of this algorithm are given in[24]. OMOPSO is a multi-objective particle swarm optimization algorithm that includes an ε-dominance archive to discover a diverse set of Pareto optimal solutions. OMOPSO was originally introduced in[25].

According to the chosen number of design parameters, more than 7000 different combinations (each combination represents an aircraft) have been generated and analyzed to define the response surface on which perform the optimization process. The Pareto front, in this optimization problem is a multidimensional frontier, according to the chosen design parameters. Targets of the optimization process have been the cruise parameter W/E, the take-off and landing factors $W/(Sw*C_{Lmax})$. To ensure the aircraft stability, a static margin of 5% has been assigned as constraint.

Fig. 32 shows an example of two objectives Pareto front for the optimization of the Configuration 1., considering the two parameters $W/(Sw*C_{Lmax})_{LND}$ and W/E_{cruise}

Fig. 33 shows the comparison between the three optimized configurations and their relative load and balance diagram. All the major results are summarized in Table 6.

To ensure the required stability, Configuration 1 is characterized by a very large horizontal tail area (S_H = 56m^2) about 51% of the wing area. This provides an increment of both the maximum take-off weight and induced drag which lead to the lowest cruise efficiency among the three solutions (17.3 as reported in Table 6.).

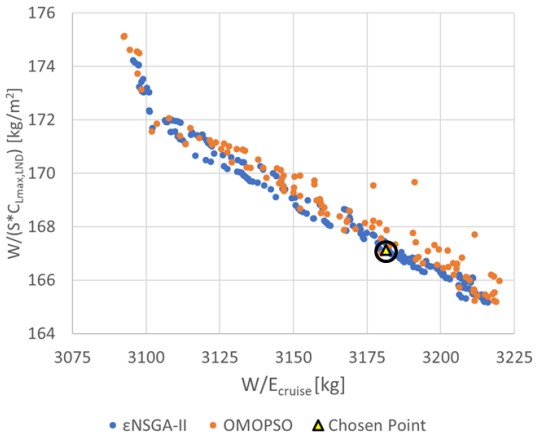

Fig. 32 Example of Pareto front for the optimization of Configuration 1.

To avoid a large horizontal tail area, a limitation on the center of gravity range has been imposed leading to the Configuration 2. This aircraft must operate within the imposed c.g. variation (11% to 40% MAC). This allows to reach a higher cruise efficiency with respect to the first configuration (E = 17.7), a lower maximum take-off weight and a slightly reduction of maximum lift coefficient in landing (see Table 6.).

The first two configurations do not meet the required cruise aerodynamic efficiency.

Configuration 3 provides a three lifting surfaces layout. In this case the wing area is reduced, and its position is back shifted. This latter leads to a c.g. range that lies forward the mean aerodynamic chord leading edge (see Fig. 33). For this aircraft, in cruise condition, it is possible to trim the aircraft with a reduced download on the horizontal tail, allowing a lower trim drag. This provides a higher cruise efficiency (18.4 with respect to 17.7 of the Configuration 2).

Moreover, the maximum achievable lift coefficients are increased thanks to the canard surface.

Fig. 34 shows the comparison between the aerodynamic efficiency at several flight conditions for all the three considered configurations at max aft c.g. position. As it can be appreciated, the canard is the solution that gives the maximum cruise efficiency being the only one configuration above the required value of 18 at C_L=0.61.

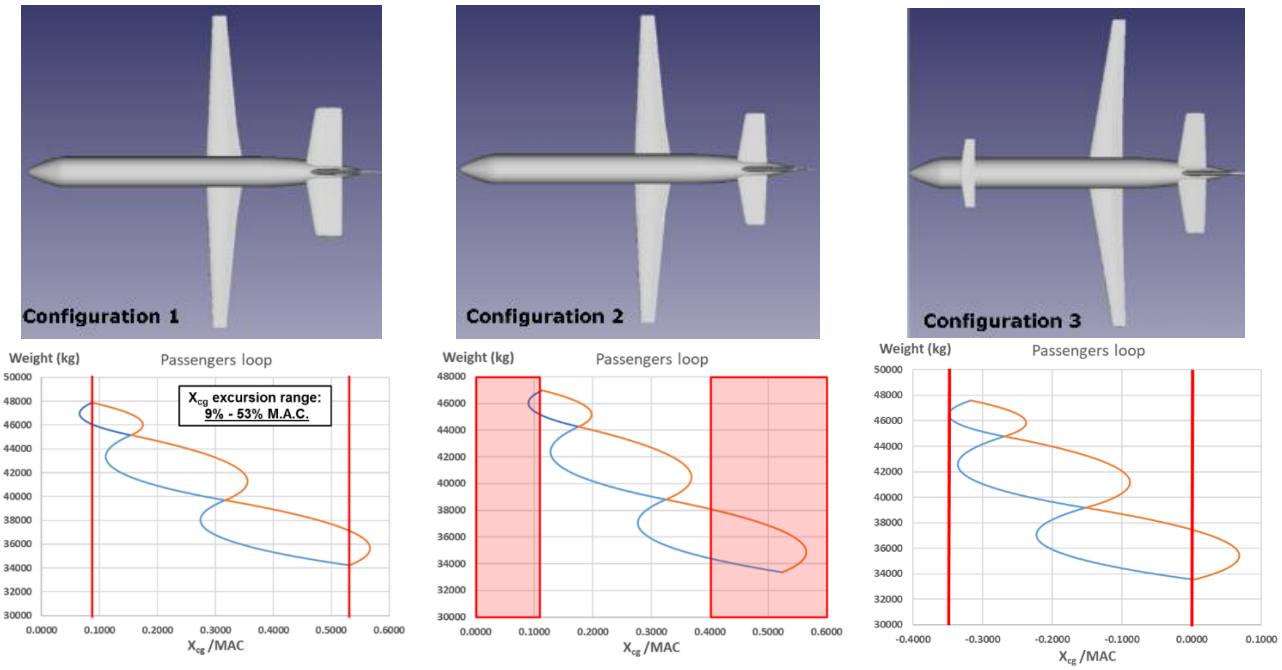

Fig. 33 Configuration comparison: planform and X_{cg} excursion.

	Loop1	Config. 1	Config. 2	Config. 3
W_{TO} (kg)	54410	54976	54105	54849
Cruise Efficiency	16.7	17.3	17.7	18.4
$C_{Lmax\ clean}$	1.53	1.70	1.70	1.91
$C_{Lmax\ TO}$	2.15	2.63	2.63	2.90
$C_{Lmax\ LND}$	2.30	3.19	3.09	3.40
S_w (m^2)	105	103	105	98.6
Max. Cruise Mach	0.61	0.63	0.64	0.66

Table 6 Configurations comparison.

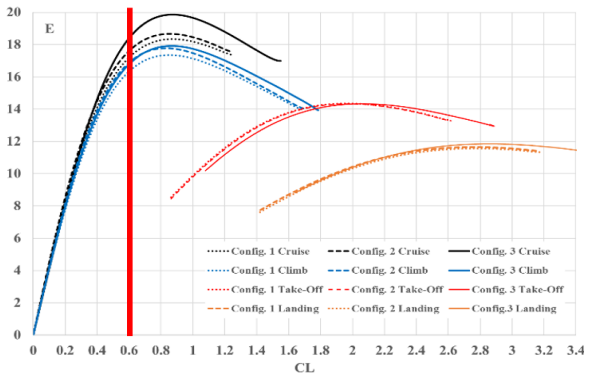

Fig. 34 Configuration Comparison: Efficiency at several flight conditions, max aft c.g.

7 Conclusions

IRON loop1 design and analysis have been performed. Laminar airfoil for cruise Mach number 0.64 has been designed, also considering high lift requirements. A very efficient single slotted fowler flap has been designed which allows promising high lift wing capabilities. Both aircraft climb and cruise performance have been improved through wing-tip devices. Winglet leads to an induced drag reduction of about 10% in climb condition compared to a wing having the same span. An accurate weight and balance analysis has shown a wide center of gravity excursion, highlighting: unstable loop1 configuration (max forward c.g.), insufficient maximum lift coefficients and a cruise efficiency lower than the required. Within loop2, the aircraft configuration revision has shown that the three-lifting surfaces is the best solution to comply with TLAR. IRON loop2 aerodynamic database will be assessed by means of high-fidelity tools, to allow aircraft performance and costs evaluation.

8 Acknowledgments

The project leading to these results (IRON project) has received funding from the Clean Sky 2 Joint Undertaking under the European Union's Horizon H2020 research and innovation program under *Grant Agreement* n° 807089 REG GAM 2018. The authors are grateful to the partners of the IRON consortium for their contributions and feedback.

References

[1] Coiro, D.P., Nicolosi, F. "Design of Low-Speed Aircraft by Numerical and Experimental Techniques Developed at DPA," Aircraft Design Journal, Vol. 4, N. 1, Pag1-18, March 2001. ISSN 1369-8869

[2] Pascale, L., Nicolosi, F. Design and aerodynamic analysis of a light twin-engine propeller aircraft, (2008) ICAS Secretariat - 26th Congress of International Council of the Aeronautical Sciences 2008, ICAS 2008, 1, pp. 3890-3904.

[3] Coiro, D.P., Nicolosi, F., Scherillo, F., Maisto, U. "Improving Hang-Glider Maneuverability using multiple winglets: a numerical and experimental investigation", Journal of Aircraft, Vol. 45, N. 3, May-June 2008, pp. 981-989, doi: 10.2514/1.33265.

[4] Coiro, D.P., Nicolosi, F. Grasso, F. "Design and Testing of Multi-Element Airfoil for Short-Takeoff-and-Landing Ultralight Aircraft", Journal of Aircraft, Vol. 46, N. 5, Sept.-Oct. 2009, pp. 1795-1807, doi: 10.2514/1.43429.

[5] Della Vecchia, P., Nicolosi, F. "Aerodynamic guidelines in the design and optimization of new regional turboprop aircraft", Aerospace Science and Technology (Elsevier) AESCTE Vol. 38, October 2014, pp. 88-104, doi: 10.1016/j.ast.2014.07.018.

[6] Della Vecchia, P., Stingo, L., Nicolosi, F., De Marco, A., Daniele E. and D'Amato, E, "Application of Game Theory and Evolutionary Algorithm to the Regional Turboprop Aircraft Wing Optimization", In Evolutionary and Deterministic Methods for Design Optimization and Control with Applications to Industrial and Societal Problems, Springer International Publishing AG, part of Springer Nature, 2019, doi:10.1007/978-3-319-89890-2_26.

[7] M. Zhang, A. Rizzi, F. Nicolosi, A. De Marco,"*Collaborative Aircraft Design Methodology using ADAS linked to CEASIOM",* 32nd AIAA Applied Aerodynamic ConferenceAtlanta, GA (USA), 16-20 June, 2014, doi:10.2514/6.2014-2012.

[8] Nicolosi, F., Della Vecchia, P., Ciliberti, D., Cusati, V., "Fuselage aerodynamic prediction methods", (2016) Aerospace Science and Technology, 55, pp. 332-343. doi: 10.1016/j.ast.2016.06.012.

[9] Ciliberti, D., Della Vecchia, P., Nicolosi, F., De Marco, A., "Aircraft directional stability and vertical tail design: A review of semi-empirical methods", (2017) Progress in Aerospace Sciences, 95, pp. 140-172. doi: 10.1016/j.paerosci.2017.11.001.

[10] Nicolosi, F., Corcione, S., Della Vecchia, P, Commuter aircraft aerodynamic characteristics through wind tunnel tests, (2016) Aircraft Engineering and Aerospace Technology, 88 (4), pp. 523-534, doi: 10.1108/AEAT-01-2015-0008.

[11] Nicolosi F., De Marco A., Della Vecchia P., Sabetta V."Roll performance assessment of a light aircraft: fight simulations and fight tests, Aerospace Science and Technology (Elsevier), Volume 76, May 2018, Pages 471-483, doi: 10.1016/j.ast.2018.01.041.

[12] Nicolosi, F., Della Vecchia, P., Corcione, S., "Design and aerodynamic analysis of a twin-engine commuter aircraft" (2015) Aerospace Science and Technology, 40, pp. 1-16. doi: 10.1016/j.ast.2014.07.018.

[13] Nicolosi, F., De Marco, A., Attanasio, L., Della Vecchia, P. "Development of a Java-based framework for aircraft preliminary design and optimization", (2016) Journal of Aerospace Information Systems, 13 (6), pp. 234-242. doi: 10.2514/1.1010404.

[14] Trifari, V., Ruocco, M., Cusati, V., Nicolosi, F., De Marco, A., "Java framework for parametric aircraft design - Ground performance", (2017) Aircraft Engineering and Aerospace Technology, 89 (4), pp. 599-608, doi: 10.1108/AEAT-11-2016-0209.

[15] Nicolosi, F., & Paduano, G. (2011). Development of a Software for Aircraft Preliminary Design and Analysis. *3rd CEAS Air & Space Conference* (pp. 702-714). Venezia (IT): CEAS.

[16] Roskam, J. (2000). *Airplane Design - Part VI: Preliminary Calculation of Aerodynamic, Thrust and Power Characteristics.* Lawrence (KS): DAR Corporation.

[17] P. Sforza; 2014; *Commercial Airplane Design Principles*; Elsevier Science.

[18] W. H. Wentz, Jr., and H. C. Seetharam, *Development of a fowler flap system for high performance general aviation airfoil*, NASA Contractor Report, NASA CR-2443, National Aeronautics and Space Administration, Washington, D.C., December 1974.

[19] M. Kintscher, M. Wiedemann and H. Monner (2011), Design of a smart leading edge, *International Journal of Structural Integrity, vol.* 2(4), pp. 383-405.

[20] Perkins, C., & Hage, R. (1949). *Airplane Performance Stability and Control.* New York: John Wiley & Sons Inc.

[21] Multhopp, H. (1942). *Aerodynamic of the Fuselage.* Technical Memorandum 1036, National Advisory Committee for Aeronautics.

[22] Munk, M. (1924). *The Aerodynamic Forces on Airship Hulls.* Technical Report 184, National Advisory Committee for Aeronautics.

[23] Torenbeek, E. (1982). *Synthesis os Subsonic Airplane Design.*Delft University Press.

[24] Kollat, J. B., and Reed, P. M. "Comparison of Multi-Objective Evolutionary Algorithms for Long-Term Monitoring Design."Advances in Water Resources, 29(6):792-807, 2006.

[25] Sierra, M. R. and Coello Coello, C. A. "Improving PSO-based multi-objective optimization using crowding, mutation and ε-dominance." Evolutionary Multi-Criterion Optimization, Berlin, Germany, 505-519, 2005.

Copyright Statement